AQUA
Water Infrastructure, Ecosystems and Society

IWA PUBLISHING

AQUA — Water Infrastructure, Ecosystems and Society Vol 71 No 7, 849 doi: 10.2166/aqua.2022.167

A fixed-bed column study of solid waste-based calcium silicate hydrate for the phosphate removal

Alemu Gizaw [a,b,*], Feleke Zewge [a], Yonas Chebude[c], Melakuu Tesfaye[b] and Andualem Mekonnen[d]

[a] Africa Center of Excellence for Water Management, Addis Ababa University, Addis Ababa, Ethiopia
[b] Department of Chemical Engineering, Adama Science and Technology University, Adama, Ethiopia
[c] Department of Chemistry, College of Natural and Computational Sciences, Addis Ababa University, Addis Ababa, Ethiopia
[d] Center for Environmental Sciences, Addis Ababa University, Addis Ababa, Ethiopia
*Corresponding author. E-mail: alemu.gizaw@aau.edu.et

AG, 0000-0002-0033-1948

ABSTRACT

The calcium silicate hydrate (CSH) was synthesized from the solid waste residue (SWR) of the Alum Factory, and was used for phosphate abatement from an aqueous solution. Fixed-bed column adsorption experiments were conducted at different flow rates (5, 7.5, and 10 mL/min) and bed depths (6, 9, and 12 cm) at an initial pH and phosphate concentrations of 5 and 5.5 mg/L, respectively. The breakthrough curve analysis was developed and tabulated for the effects of the flow rate and bed depth. Fixed-bed adsorption models, namely the Thomas model, the Yoon–Nelson model, and Bed Depth Service Time (BDST) model were fitted to the experimental data. The R^2 values observed for the Thomas model and the Yoon–Nelson model were 0.96 and 0.98, respectively, at the flow rate of 7.5 mL/min and bed depth of 9 cm with the breakthrough adsorption capacity of 5.67 mg/g. The synthesized CSH was also tested for its phosphate removal efficiency using local wastewater treatment plant effluent. About 1,658 mL of real wastewater was treated for 249 min before the standard threshold limit (1 mg/L) was reached. This study prevails that the synthesized CSH could be applied to remove phosphate from real wastewater under a continuous flow adsorption system.

Key words: adsorption, breakthrough curve, calcium silicate hydrate, fixed-bed column, phosphate abatement

HIGHLIGHTS

- Calcium silicate hydrate (CSH) is used to remove phosphate from the aqueous solution under a continuous flow system.
- Breakthrough curves were developed at different flow rates and bed depths.
- The Thomas model, Yoon–Nelson model, and bed depth service time (BDST) model were applied to the experimental data.
- The breakthrough bed capacity observed for CSH adsorbent was 5.67 mg/g.

GRAPHICAL ABSTRACT

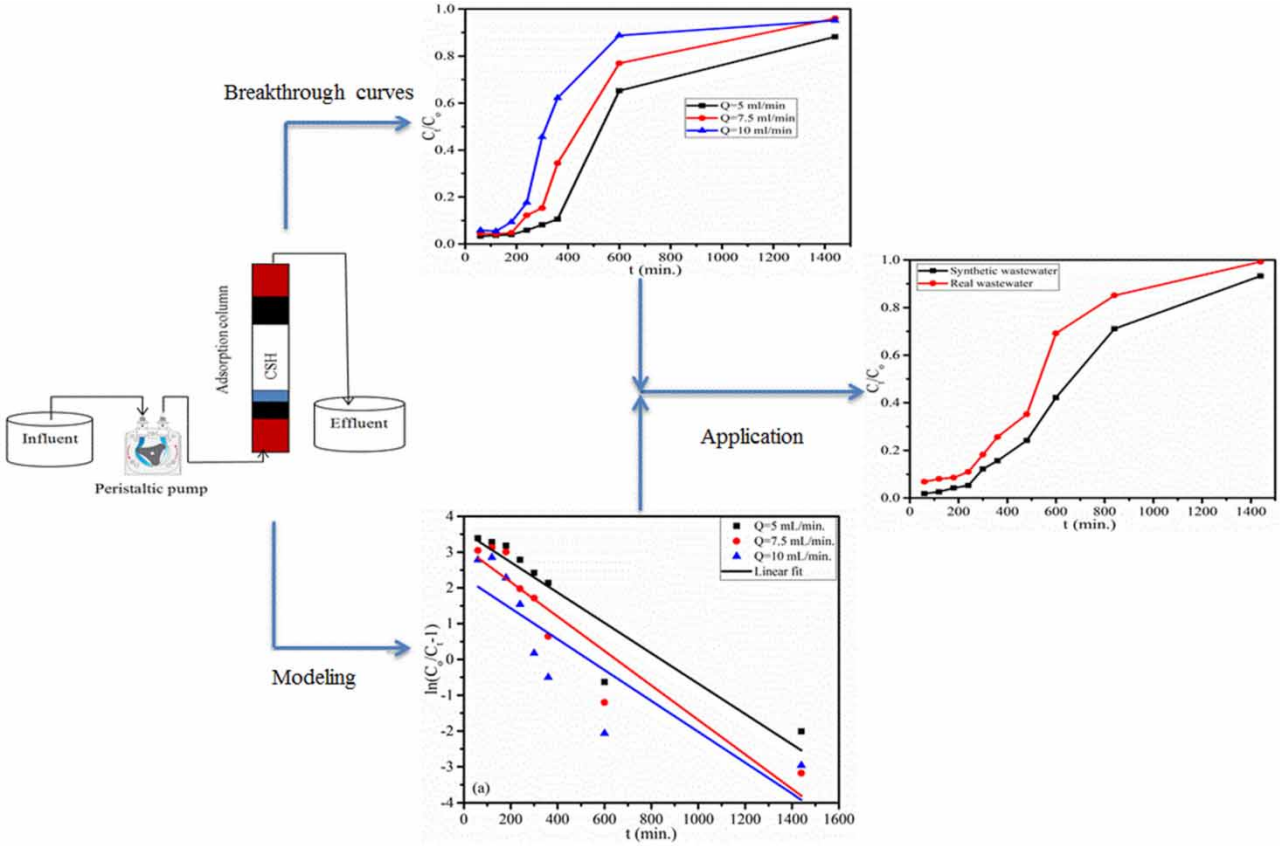

1. INTRODUCTION

Phosphorous is one of the essential and highly required nutrients for the plant growth that is difficult to be substituted (Berg *et al.* 2007). Various mechanisms have been developed to deliver this nutrient to the plant. However, a significant amount of phosphorus-containing nutrients is lost to different streams such as leaching into water bodies, which is capable of causing a problem for the aquatic life. The phosphorous concentration above 0.02 mg/L was reported to cause eutrophication (Nguyen *et al.* 2015). Therefore, it is very important to control the phosphate discharge level to suppress the problem related to eutrophication. To regulate this problem, different discharge limit standards were developed by different concerned organizations. In most conditions, the discharge limits are in the range of 0.5–1 mg/L implying that the removal of phosphate from wastewater before discharging into any water bodies is not optional but rather obligatory (Nguyen *et al.* 2015). Phosphate can be removed using different conventional and easily manageable technologies such as enhanced biological reactors, wetland, membrane technologies, electrochemical processes, chemical precipitation, and adsorption (Monfet *et al.* 2017; Prashantha Kumar *et al.* 2018). Various researchers reported that adsorption is an attractive and prominent technology for the removal of phosphate from wastewater. It is efficient, easy, fast, environmentally friendly, and can be considered a low-cost method (Liu *et al.* 2018).

Recently, numerous modified adsorbents were reported for phosphate removal. Most of them were derived from agricultural and industrial by-products. Meat and bone meal incineration ash (Leng *et al.* 2019), calcium-decorated biochar (Wang *et al.* 2018), lanthanum-loaded zeolite beads (Pham *et al.* 2019), and $La(OH)_3/Fe_3O_4$ nanocomposites (Wu *et al.* 2017) were few among the top reported phosphate adsorbents (Gizaw *et al.* 2021a). However, the studies of the adsorption system of the aforementioned adsorbents were limited to the batch mode. Batch mode experiments are time-consuming and their generated data do not represent the real nature of the process and are very limited to scale-up. On the other hand, a continuous mode of operation has a benefit in treating a large quantity of influent. It is ease for scale-up using the

experimental data, efficient, and reduce adsorbent consumption (Nguyen *et al.* 2015). To gain these advantages, the continuous mode of operation such as fixed-bed column adsorption is attracting different researchers. Considerable phosphate removals from an aqueous solution have been reported by applying a fixed-bed column adsorption using adsorbents such as Ca-impregnated lignite (Samaraweera *et al.* 2021), granular acid-activated red mud (Hu *et al.* 2019), lime-iron sludge (Chittoo & Sutherland 2020), slag filter media (Lee *et al.* 2015), biochar-calcium alginate beads (Jung *et al.* 2017a), steel by-products (Sellner *et al.* 2019), electromagnetic modified calcium alginate beads (Jung *et al.* 2017b), and chitosan/Ca-organically modified beads (Jang & Lee 2019).

Moreover, kaolin clay, which is quite similar in its silica composition to the solid waste residue (SWR) used in this work to synthesize calcium silicate hydrate (CSH) (Gizaw *et al.* 2021b), was reported as a low-cost water filter mixed with jute fibers at different compositions (Hussain & Al-Fatlawi 2020). According to Hussain & Al-Fatlawi (2020), this developed filter effectively remove total hardness, magnesium, potassium, calcium, chloride alkalinity, and other similar.

In this study, CSH was synthesized from the SWR of the Alum Factory which was reported as hazardous waste due to its acidic nature (Nigussie *et al.* 2007). A substantial amount of this SWR was dumped around the factory and there were no reported economically feasible methods to reuse or dispose of it. The solid waste is composed of a high content of silica, which is a promising precursor to produce CSH. CSH is well known as an adsorbent and has been used as a crystal seed, calcium ion donor for the formation of hydroxyapatite when it is exposed to phosphate-containing solutions and self-adjust the pH during the phosphate adsorption process which makes it preferable for the phosphate removal (Kuwahara & Yamashita 2017; Zhang *et al.* 2019). The first novelty of this work is the reuse and economic value addition of this SWR of the Alum Factory. Second, to the extent of our review conducted, there was no reported work on the CSH synthesized from such toxic and low-cost silicate material through the sol–gel method.

A preliminary batch adsorption study using the synthesized CSH has shown remarkable phosphate removal. Inspired by this observation, this work was developed to investigate the breakthrough curve for the factors affecting fixed-bed adsorption column, namely depth and flow rate followed by modeling of the adsorption process using commonly reported models, namely the Thomas model, Yoon–Nelson model, and Bed Depth Service Time (BDST) model. The adsorption capacity of the synthesized CSH was compared with the similar works reported by different scholars. Finally, the practical application of the synthesized CSH on the wastewater collected from a local municipal wastewater treatment plant was presented.

2. MATERIALS AND METHODS

2.1. Materials

The CSH was synthesized from the SWR of the Alum Factory by the sol–gel method, and used as an adsorbent (Gizaw *et al.* 2021b). Calcium chloride ($CaCl_2$) was used as a source of calcium ions in the synthesis. Potassium dihydrogen orthophosphate (KH_2PO_4) was used to prepare a phosphate stock solution of 1,000 mg/L. Hydrochloric acid (HCl) and sodium hydroxide (NaOH) was used to adjust the pH of the solution. The phosver® 3 powder pillow phosphate reagent was used to measure phosphate concentration at 880 nm using a UV–Vis DR6000 spectrophotometer (Hach DR6000TM, LPV441.99.00002, USA). The real wastewater samples were taken from the effluent sampling point of the Kality wastewater treatment plant (KWWTP) located in Addis Ababa, Ethiopia; and were stored at 4 °C. The physicochemical analysis of this wastewater was reported in the previous work (Gizaw *et al.* 2021b).

2.2. Fixed-bed column adsorption experimental setup

A glass with an internal diameter (ID 2.8 cm), outer diameter (OD 3 cm), and total depth (H 23 cm) was used as the adsorption column. A drilled rubber stopper was fitted on both ends. This rubber stopper was used as a cap, and to connect influent and effluent streams to the column. The glass wool was placed on the bottom and top to avoid the CSH adsorbent washout. Moreover, inert glass beads were packed in the bottom aiming to direct the influent uniformly throughout the column. A peristaltic pump was used to uniformly feed the influent to the column in the up-flow direction to safeguard better adsorbent–adsorbate contact (Figure 1). The experiments were conducted at room temperature. The influent phosphate concentration and initial pH used were 5.5 mg/L and 5, respectively. These values were pre-determined optimum values using batch experiments. The influent stream was passed through the column at different flow rates of 5, 7.5, and 10 mL/min to evaluate the effect of flow rates on phosphate adsorption. The effect of column depth was also evaluated by operating the adsorption column at different depths and keeping the flow rate constant. In this work, 5.26, 7.7, and 9.9 g CSH adsorbent was packed in the column to obtain the corresponding depth of 6, 9, and 12 cm, respectively. The synthesized CSH was applied

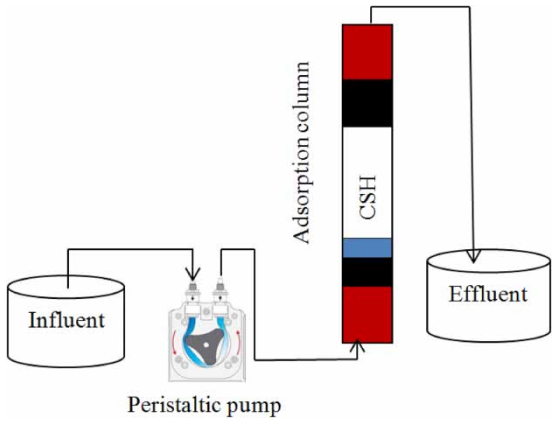

Figure 1 | Systemic flow chart diagram of a fixed-bed adsorption column: rubber stopper (red shaded); glass wool (black shaded); glass beads (blue shaded). Please refer to the online version of this paper to see this figure in color: http://dx.doi.org/10.2166/nh.2022.018.

to remove phosphate from real wastewater at the optimum flow rate, and depth. The duplicate ($n = 2$) experiments were conducted and maximum errors tolerated were settled at 0.05 or 5%. The maximum error observed in this work was 0.031 or 3.1%. The fixed-bed column adsorption models were evaluated based on their R^2 value generated from the model linear fit. These values were compared for best-fit selection.

A 10 mL of sample was collected from the effluent at a different time interval and analyzed for its phosphate concentration using DR 6000 spectrophotometer.

2.3. Breakthrough analysis

The dynamic performance of the fixed-bed column adsorption was analyzed by using the breakthrough curve parameters. Mainly the breakthrough curve parameters are subjected to initial adsorbate concentration, depth of the column, and flow rate. Systematic determination of these parameters helps to evaluate the column performance, and scale it up for practical applications (Golie & Upadhyayula 2016). The time taken by the column to reach the maximum threshold limit or treatment objective for phosphate effluent concentration is considered the breakthrough time (t_b) whereas exhaustion time (t_e) is the time required to obtain the phosphate effluent concentration compared with the initial concentration. The total mass of adsorbed phosphate (q_t) can be correlated with the flow rate (Q) and initial phosphate concentration as indicated by Equations (1) and (2) (Golie & Upadhyayula 2016; Du *et al.* 2018):

$$q_t = \frac{Q}{1000} \int_{t=0}^{t=t_e} C_{ad} dt \tag{1}$$

The phosphate concentration difference (C_{ad}) in Equation (1) is calculated as (Ramirez *et al.* 2018):

$$C_{ad} = C_o - C_t = C_o \left(1 - \frac{C_t}{C_o}\right) \tag{2}$$

A more generalized equation (Equation (3)) can be developed for the total mass of adsorbed phosphate by substituting Equation (2) in Equation (1) and rearranging it (Golie & Upadhyayula 2016):

$$q_t = \frac{QC_o}{1000} \int_{t=0}^{t=t_e} \left(1 - \frac{C_t}{C_o}\right) dt \tag{3}$$

The fixed-bed column adsorption capacity (q_m) (mg/g) with the given time interval for the mass of packed adsorbent (M) (g) is defined as (Ramirez *et al.* 2018):

$$q_m = \frac{q_t}{M} \tag{4}$$

For the fixed-bed column adsorption, the efficiency is usually determined by using the mass transfer zone length (MTZ, cm) on the adsorbent layer where 10–90% of the influent concentration changes to effluent concentration, which is expressed as Equation (5) (Lee *et al.* 2015):

$$MTZ = H\frac{(t_e - t_b)}{t_e} \tag{5}$$

where H is the depth of the bed volume.

Moreover, the total amount of phosphate entering the column (W_t, g), the percentage removal (R, %) of the column, the total effluent volume (V_e, mL), and total breakthrough volume (V_b, mL) can be also estimated by applying Equations (6)–(9), respectively (Reinhardt *et al.* 2021).

$$W_t = C_o Q t_e \tag{6}$$

$$R(\%) = \frac{(q_t)}{W_t} \times 100 \tag{7}$$

$$V_e = Q t_e \tag{8}$$

$$V_b = Q t_b \tag{9}$$

2.4. A fixed-bed column adsorption kinetic model

2.4.1. The Thomas model

This model is one of the common models used for the evaluation of fixed-bed column adsorption operation. It is applied to assess the column adsorption rate constant and adsorption capacity using the equation described as follows (Nguyen *et al.* 2015; Reinhardt *et al.* 2021):

$$\ln\left(\frac{C_o}{C_t} - 1\right) = \frac{k_{Th} q_m M}{Q} - k_{Th} C_o t \tag{10}$$

where k_{Th}, q_m, M, Q, C_o, C_t, and t are Thomas model rate constants (mL/min mg), adsorption capacity (mg/g), adsorbent mass (g), flow rate (mL/min), influent phosphate concentration (mg/L), effluent phosphate concentration (mg/L) at the given time, and column operation time (min), respectively. The linear plot of $\ln(C_o/C_t - 1)$ versus t was used to determine the values of k_{Th} and q_m.

2.4.2. The Yoon–Nelson model

The Yoon–Nelson kinetic model is the simplest model applied to estimate the exhaustion time and the behavior of the adsorption process toward phosphate concentration. The Yoon–Nelson kinetic model is expressed as (Li *et al.* 2013; Woumfo *et al.* 2015):

$$\ln\left(\frac{C_t}{C_o - C_t}\right) = k_{YN} t - \tau k_{YN} \tag{11}$$

where k_{YN} and τ are rate constants (mL/mg·min), and the time required for the 50% phosphate breakthrough (min). The linear plot of $\ln[C_t/(C_o - C_t)]$ versus time helps to determine k_{YN} and τ, respectively, from the slope, and intercept of the plot.

2.4.3. The BDST model

This model relates the column bed depth with the column service time. The linear equation of BDST is given as (Golie & Upadhyayula 2016):

$$t = \frac{ZN_o}{C_o v} - \frac{1}{k_b C_o} \ln\left(\frac{C_o}{C_b} - 1\right) \tag{12}$$

where t, Z, C_o, C_b, N_o, k_b, and v stands for column service time (min), bed depth (cm), influent phosphate concentration (mg/L), effluent phosphate concentration (mg/L), saturation concentration (mg/L), rate constant (mL/mg·min), and linear velocity (flow rate divided by area of the column) (cm/min), respectively. From the linear plot of time versus column bed depth, the slope and intercept of the plot can be used to determine N_o and k_b, respectively. From Equation (12), the critical bed depth (Z_o, cm) required to obtain the targeted effluent phosphate concentration (C_b) can be calculated by setting $t = 0$ and expressed as shown in Equation (13) (Berg *et al.* 2007).

$$Z_o = \frac{v}{k_b N_o} - \ln\left(\frac{C_o}{C_b} - 1\right) \tag{13}$$

3. RESULTS AND DISCUSSION

3.1. Effects of fixed-bed adsorption parameters

3.1.1. Effect of the flow rate

As illustrated in Figure 2, the breakthrough time ($C_t/C_o = 0.1$) and exhaustion time ($C_t/C_o = 0.9$) were observed to decrease from 354 to 188 min and from 1,469 to 783 min, respectively, as the flow rate increased from 5 to 10 mL/min. This is probably due to the increment in the flow rate allowing more quantity of influent to pass through the column which in turn drives more phosphate ions to be exposed to the active sites of CSH. Due to this reason, the breakthrough time and exhaustion time are observed to decrease (Jang & Lee 2019). As shown in Table 1, higher adsorption capacity, breakthrough volume, exhaustion volume, and extended mass transfer zone were observed at a lower influent flow rate (5 mL/min). It is depicting the fact that the reduction in flow rate, decreases the turbulence that favors adsorbent–adsorbate interaction and increases the influent residence time in the column that allows the system to reach the equilibrium before the phosphate exit the column (Nuryadin & Imai 2021). Similar results were previously reported by Pap *et al.* (2020), Pap *et al.* (2020) and Ye *et al.* (2021). In contrast, according to Du *et al.* (2018), a very low flow rate might result from the back mixing flow and decreases the removal efficiency of the phosphate. Based on this, a flow rate of 7.5 mL/min was selected for further investigation of different parameters in the subsequent experiments.

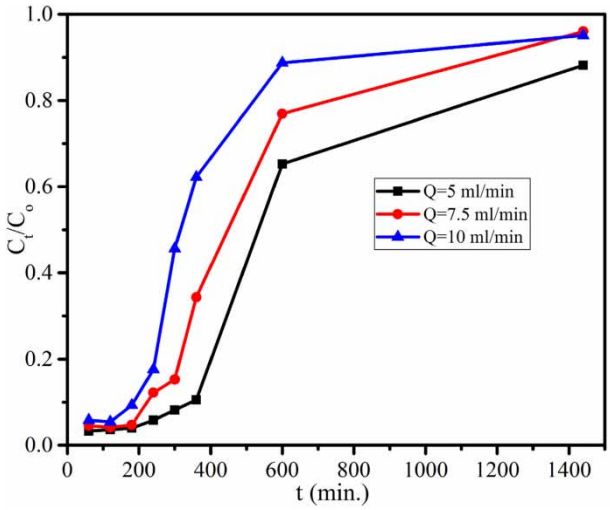

Figure 2 | Effect of the flow rate on the breakthrough curve for phosphate adsorption using CSH (bed depth = 6 cm, initial pH = 5, initial phosphate concentration = 5.5 mg/L).

Table 1 | Breakthrough curve parameter value of fixed-bed column adsorption for CSH adsorbent

Q (mL/min)	Z (cm)	t_b (min)	V_b (mL)	q_b (mg/g)	R_b (%)	t_e (min)	V_e (mL)	q_e (mg/g)	MTZ (cm)
5	6	354	1,769.9	1.96	88.9	1,469	7,346.1	8.8	4.9
7.5	6	227	1,700.6	1.85	91.4	1,186	8,892.8	7.8	4.6
10	6	188	1,877.6	1.78	90.5	783	7,831.7	7.3	4.6
7.5	6	134	1,005.5	1.0	92.7	1,155	8,661.9	6.0	5.3
7.5	9	288	2,162.3	1.32	94.1	1,344	10,080.4	7.1	7.1
7.5	12	319	2,393.1	1.53	96.3	1,447	10,849.9	8.6	9.4

3.1.2. Effect of the depth

The effect of the adsorption column depth on the phosphate removal by the CSH is presented in Figure 3. As clearly indicated, both breakthrough time and exhaustion time increases from 134 to 319 min and from 1,155 to 1,447 min, respectively, as the bed depth increased from 6 to 12 cm (Table 1). The result is also in line with other previously reported articles which confirm an increase in fixed-bed column adsorption service time with the bed depth increase (Berg *et al.* 2007; Golie & Upadhyayula 2016). The observed wider mass transfer zone for the phosphate adsorption (Figure 3) is mainly correlated to the flatness of the breakthrough curve with the increment of depth that in turn results in the extended mass transfer zone (Ramirez *et al.* 2018). Similarly, the breakthrough volume and exhaustion volume increased from 1,006 to 2,393 mL and from 8,662 to 10,850 mL, respectively. This is due to the extended service time, which allows more quantity of influent to pass through the column. It is commonly known that the increment in bed depth gives the privilege to increase the amount of CSH to be packed in the column that in turn increases the available active sites for the phosphate adsorption (Li *et al.* 2013; Jang & Lee 2019). This phenomenon can play a major role in the performance of the fixed-bed column adsorption by affecting the breakthrough and exhaustion adsorption capacity. Due to this reason, the breakthrough and exhaustion adsorption capacity was observed to increase from 1 to 1.53 mg/g and from 6 to 8.6 mg/g, respectively. In addition, the adsorption capacity increased with the bed depth since it provides sufficient residential time for adsorption (Singh *et al.* 2017; Pap *et al.* 2020). It is in line with the observation reported by Nguyen *et al.* (2015) for zirconium-Loaded Okara in a packed fixed-bed column for phosphate removal which is further supported by other researchers (Li *et al.* 2013; Gizaw *et al.* 2021b; Ye *et al.* 2021). However, the bed depth increment can be considered as a reason for the high possibility of bed resistance and pressure drop increase increment (Ye *et al.* 2020), and hence 9 cm for bed depth was selected for the subsequent experiments.

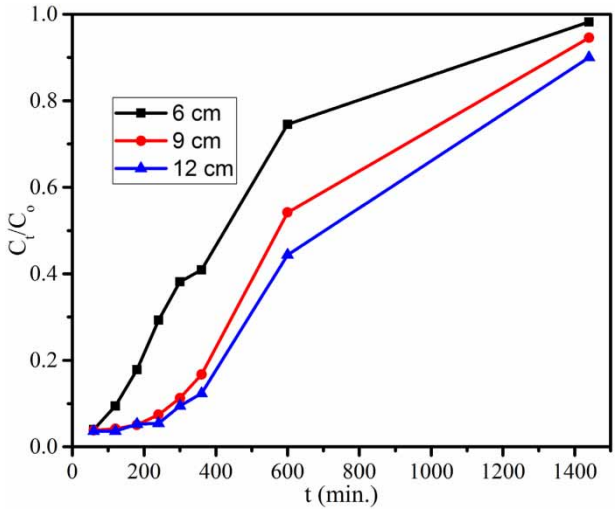

Figure 3 | Effect of the bed depth on the breakthrough curve for phosphate adsorption using CSH (flow rate = 7.5 mL/min, initial pH = 5, initial phosphate concentration = 5.5 mg/L).

3.2. Fixed-bed adsorption model results

3.2.1. The Thomas model

The plot of the Thomas model is given in Figure 4(a) and 4(b). The values of q_m and k_{Th} determined for all experimental observations are summarized in Table 2. As depicted in the aforementioned table, the value of q_m decreased from 5.49 to 1.79 mg/g. The value k_{Th} kept increasing from 0.77×10^{-3} to 0.88×10^{-3} mL/mg·min with the flow rate increment from 5 to 10 mL/min. This is because an increase in flow rate shortens the contact time between the phosphate ions and CSH active sites (Rout *et al.* 2017). A quite similar trend between the flow rate and q_m and k_{Th} was reported by Jung *et al.* (2017a) using biochar-calcium alginate beads. Moreover, Table 2 indicates that an increase in the fixed-bed column adsorption depth from 6 to 12 cm at a constant flow rate, decreases the values of k_{Th} and increases the value of q_m. The possible reason for this might be the phosphate concentration gradient formed between CSH and influent, which is mainly used as the driving force for the adsorption. This is in good agreement with reported results by different researchers (Sun *et al.* 2014; Rout *et al.* 2017). As shown in Table 2, the highest correlation coefficient (R^2) is found at the flow rate of 7.5 mL/min and a depth of 9 cm for the Thomas model, and these values are used in the subsequent experiments (Figure 4(b)).

3.2.2. The Yoon–Nelson model

The plot of the Yoon–Nelson model is given in Figure 5 and Table 2 supports the numeric results. As the influent flow rate increased from 5 to 10 mL/min, the value of the k_{YN} parameter increased from 4.24×10^{-3} to 4.82×10^{-3} min^{-1} whereas the τ value is observed to decrease from 792 to 532 min. An increase in the influent flow rate allows more phosphate to pass through the fixed-bed column adsorption within a short period and thus the CSH adsorbent is saturated quickly (Babu & Gupta 2005; Li *et al.* 2013). Consequently, the 50% breakthrough time (τ) is decreased. In contrast, when the bed depth

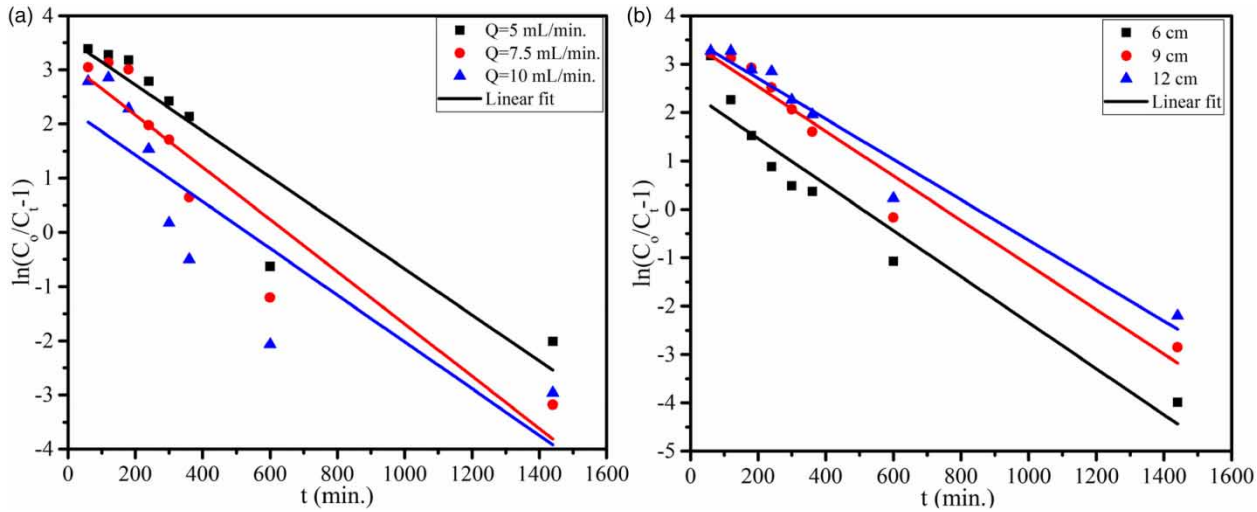

Figure 4 | The Thomas model for phosphate adsorption using CSH: (a) bed depth = 9 cm, initial pH = 5, initial phosphate concentration = 5.5 mg/L; (b) flow rate = 7.5 mL/min, initial pH = 5, initial phosphate concentration = 5.5 mg/L.

Table 2 | Fixed-bed column adsorption model constant for CSH adsorbent

Parameter		Thomas			Yoon–Nelson		
Q (mL/min)	Z (cm)	$k_{Th} \times 10^{-3}$ (mL/mg·min)	q_m (mg/g)	R^2	$k_{YN} \times 10^{-3}$ (min^{-1})	τ	R^2
5	6	0.77	5.49	0.795	4.24	791.89	0.795
7.5	6	0.78	4.13	0.872	4.31	649.27	0.872
10	6	0.88	1.79	0.865	4.82	531.95	0.865
7.5	6	0.86	2.24	0.918	4.76	507.77	0.918
7.5	9	0.84	5.67	0.960	4.61	749.46	0.983
7.5	12	0.76	5.62	0.958	4.18	847.13	0.982

increased from 6 to 12 cm, k_{YN} reduced from 4.76×10^{-3} to 4.18×10^{-3} min^{-1} and τ increased from 508 to 847 min. This describes the fact that with increasing the bed depth, a high amount of CSH was used to pack and gives more active sites for the phosphate adsorption, which in turn decreases the k_{YN} values, and elevated τ (Nuryadin & Imai 2021). For this model, the highest R^2 value (0.96) is observed at the flow rate of 7.5 mL/min and a bed depth of 9 cm (Figure 5(b)). Another study also reported a similar observation (Ramirez *et al.* 2018).

3.2.3. The BDST model

Figure 6 demonstrates the relationship between service time and depth for phosphate adsorption using CSH. For the constant depth, smaller breakthrough points (%) require a shorter service time compared to higher breakthrough points (Figure 6). This result is in good agreement with previous research reports (He *et al.* 2016). Table 3 illustrated the BDST model parameters (N_o, k_b) and the smallest bed depth required for the end-user at the settled desired breakthrough concentration (C_b) with phosphate initial concentration of 5.5 mg/L and influent flow rate of 7.5 mL/min. High correction coefficients (R^2) of 0.959, 0.962, 0.972, 0.988, and 0.998 are observed, respectively, for breakthrough points of 10, 20, 30, 40, and 50%, in column service time versus depth. It could depict that the model could be used to predict the breakthrough time (t_b) required for the targeted bed depth without conducting an extra experiment.

3.3. Adsorption–desorption test

According to Ateia *et al.* (2020), adsorption reversibility study is very important for the new adsorbent to propose for practical use. The exhausted CSH was washed by passing the 0.5 M NaOH solution through the bed for 30 min at 7.5 mL/min. Following this, the bed was washed using deionized water at the same time and flow rate. This step was repeatedly done for each cycle. The phosphate removal efficiency of 91, 83.4, 63, 37.6, and 33.3% was observed for the first, second, third, fourth, and fifth adsorption–desorption cycles, respectively (Figure 7). As indicated in Figure 7, the CSH could have successfully removed phosphate in the first two cycles and more than 50% in the third cycle. This confirmed that CSH could be used repeatedly and could be advised for cost-wise practical use.

3.4. Application using real wastewater

As already mentioned above, the application of the synthesized CSH is checked using real wastewater, which is collected from the KWWTP, located in Addis Ababa, Ethiopia. The effluent from this local wastewater treatment plant was characterized for its physicochemical parameters before the column study. After 24 h settlement, effluent wastewater was filtered using 0.45 μm filter paper. The physicochemical composition of this wastewater was pH 7.63, COD 391 mg/L, BOD 255.1 mg/L, TSS 109.2 mg/L, SO_4^{2-} 17.5 mg/L, PO_4^{3-} 5.5 mg/L, NO_3^- 21.3 mg/L, conductivity 778 μs/cm, and alkalinity 303 mg/L. According to Nguyen *et al.* (2015), 1 mg/L of phosphate discharge limit from the effluent sewage treatment plant is reported.

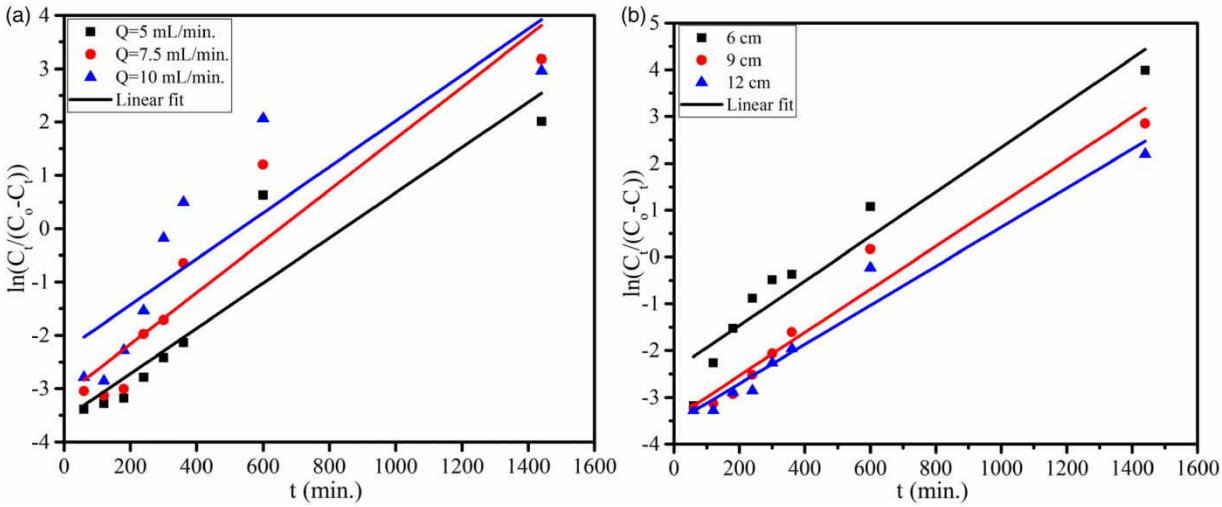

Figure 5 | Yoon–Nelson model for phosphate adsorption using CSH: (a) bed depth = 9 cm, initial pH = 5, initial phosphate concentration = 5.5 mg/L; (b) flow rate = 7.5 mL/min, initial pH = 5, initial phosphate concentration = 5.5 mg/L.

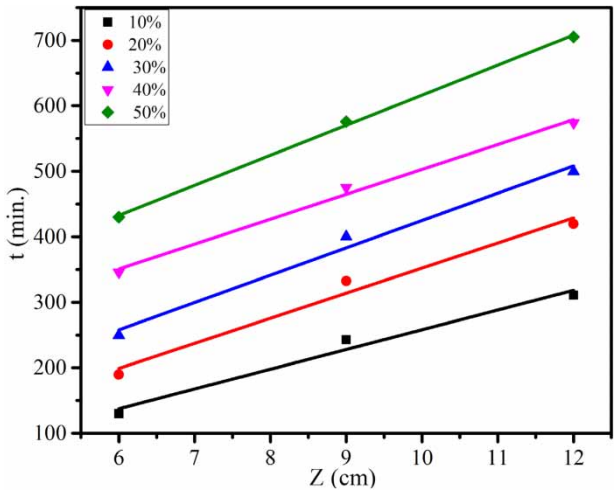

Figure 6 | The BDST model for different breakthrough points (initial pH = 5, initial phosphate concentration = 5.5 mg/L, flow rate = 7.5 mL/min).

Table 3 | Parameter values for the BDST model

Breakthrough points (%)	N_o (mg/L)	k_b (L/mg·min)	R^2
10	299.5091	0.278205	0.9594
20	380.4863	0.24755	0.9622
30	414.4552	0.61291	0.9719
40	377.6519	0.01818	0.9883
50	455.7948	0.01818	0.9975

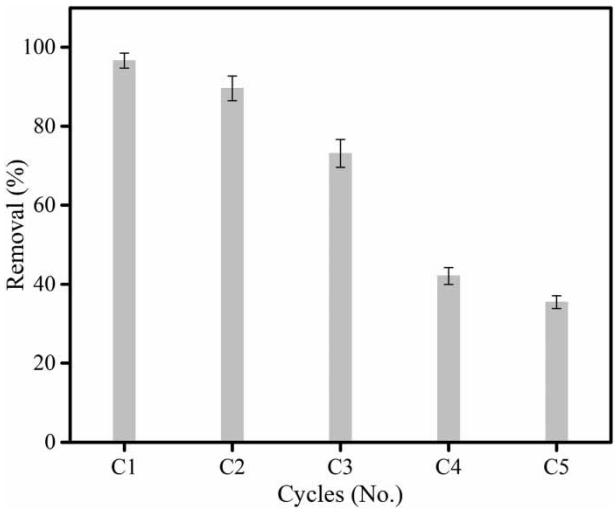

Figure 7 | The adsorption–desorption test for phosphate (initial pH = 5, flow rate = 7.5 mL/min, Z = 9 cm, initial phosphate concentration = 5.5 mg/L).

Figure 8 indicates that breakthrough time and exhaustion time for the real wastewater are obtained to be 221 and 1,056 min, respectively, whereas 286 and 1,348 min were observed for synthetic wastewater. Moreover, the fixed-adsorption column can be operated for about 249 min using real wastewater and 327 min using synthetic wastewater before the effluent phosphate concentration reached 1 mg/L, which is the recommended threshold limit for phosphate concentration in wastewater effluent stream (Nguyen *et al.* 2015). About 1,658 mL of real wastewater has been treated before it reached the threshold limit (Figure 8). The earlier time observed for the real wastewater compared to the synthetic wastewater is due to the high alkalinity and TSS, which was observed to impede the phosphate adsorption during the batch study using CSH adsorbent. This result is quite similar to the observation of previous research conducted by Sun *et al.* (2014) using Mg_3–Fe-layered double hydroxides to remove phosphate from municipal wastewater. Other researchers also reported results in good agreement with work (Husein *et al.* 2017; Sellner *et al.* 2019). This study has shown that the synthesized CSH could be applied to remove phosphate from real wastewater under a continuous flow adsorption system.

3.5. Comparison of fixed-bed adsorption capacity of CSH

The breakthrough adsorption capacity (q_b) of the synthesized CSH compared with similar reported works. As indicated in Table 4, the obtained (q_b, mg/g) using the fixed-bed column adsorption of this study is comparable to removing phosphate from an aqueous solution with a low initial phosphate concentration.

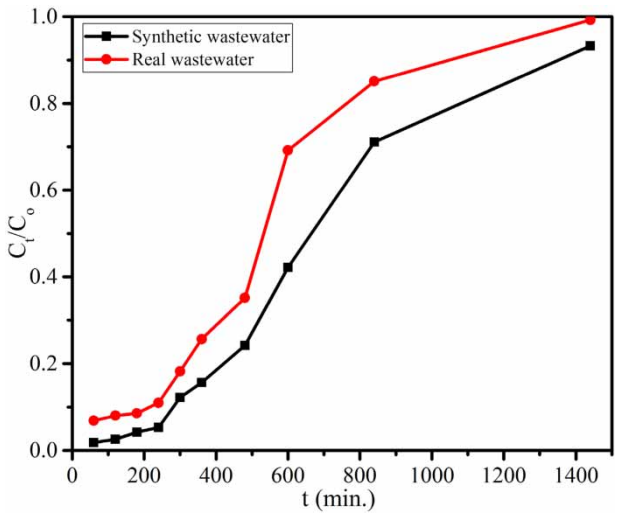

Figure 8 | A breakthrough curve for phosphate adsorption comparison for real wastewater and synthetic wastewater using CSH (bed depth = 9 cm, flow rate = 7.5 mL/min, initial pH = 7.63, initial phosphate concentration = 5.5 mg/L).

Table 4 | Comparison of fixed-bed column adsorption capacity of CSH with similarly reported adsorbents

Adsorbent	C_o (mg/L)	q_b (mg/g)	Ref.
Pyrolyzed Ca-impregnated lignite	46.6	19.5	Samaraweera *et al.* (2021)
Granular acid-activated neutralized red mud	100	68.62	Hu *et al.* (2019)
Lime-iron sludge	10.5	2.49	Chittoo & Sutherland (2020)
Slag filter media	2	0.017	Lee *et al.* (2015)
Biochar-calcium alginate beads	10	1.97	Jung *et al.* (2017a)
Recycled steel by-products	10	8.43	Sellner *et al.* (2019)
Alginate-/zirconium-grafted newspaper pellets	20	5.59	Husein *et al.* (2017)
CSH	5.5	5.67	This study

4. CONCLUSION

In this work, CSH was used to remove phosphate in the continuous adsorption system. It was observed that breakthrough time ($C_t/C_o = 0.1$) and exhaustion time ($C_t/C_o = 0.9$) decreased as the flow rate increased. The higher adsorption capacity, higher breakthrough volume and exhaustion volume, and extended mass transfer zone were observed at a lower influent flow rate (5 mL/min). As the bed depth increases, both breakthrough time and exhaustion time increase. The breakthrough and exhaustion adsorption capacity also increased with depth. For both Thomas and Yoon–Nelson models, the highest R^2 was observed at a flow rate of 7.5 mL/min and a bed depth of 9 cm. The synthesized CSH is also applied to remove phosphate from local municipal wastewater treatment plant effluent. Earlier breakthrough and exhaustion time were observed for the real wastewater as compared to the synthetic wastewater, which is due to the impeding phosphate adsorption subjected to its physicochemical characteristics. However, about 1,700 mL of real wastewater could be treated in 249 min before the threshold limit (1 mg/L) is reached. This study shows that the synthesized CSH could be applied to remove phosphate from real wastewater under a continuous flow adsorption system.

ACKNOWLEDGEMENTS

This work was financially supported by the Africa Center of Excellence for Water Management, Addis Ababa University, Ethiopia; Grant code GSR/9813/11.

DATA AVAILABILITY STATEMENT

All relevant data are included in the paper or its Supplementary Information.

CONFLICT OF INTEREST

The authors declare there is no conflict.

REFERENCES

Ateia, M., Helbling, D. E. & Dichtel, W. R. 2020 Best practices for evaluating new materials as adsorbents for water treatment. *ACS Mater. Lett.* **2**, 1532–1544. https://doi.org/10.1021/acsmaterialslett.0c00414.

Babu, B. V. & Gupta, S. 2005 Modeling and simulation of fixed bed adsorption column: effect of velocity variation. *I-Manager's J. Futur. Eng. Technol.* **1**, 60–66. https://doi.org/10.26634/jfet.1.1.966.

Berg, U., Ehbrecht, A., Röhm, E., Weidler, P. G. & Nüesch, R. 2007 Impact of calcite on phosphorus removal and recovery from wastewater using CSH-filled fixed bed filters. *J. Residuals Sci. Technol.* **4**, 73–81.

Chittoo, B. S. & Sutherland, C. 2020 Column breakthrough studies for the removal and recovery of phosphate by lime-iron sludge : modeling and optimization using artificial neural network and adaptive neuro-fuzzy inference system. *Chinese J. Chem. Eng.* **28**, 1847–1859. https://doi.org/10.1016/j.cjche.2020.02.022.

Du, Z., Zheng, T. & Wang, P. 2018 Experimental and modeling studies on fixed-bed adsorption for Cu(II) removal from aqueous solution by carboxyl modified jute fiber. *Powder Technol.* **338**, 952–959. https://doi.org/10.1016/j.powtec.2018.06.015.

Gizaw, A., Zewge, F., Kumar, A., Mekonnen, A. & Tesfaye, M. 2021a A comprehensive review on nitrate and phosphate removal and recovery from aqueous solutions by adsorption. *J. Water Supply Res. Technol.* **00**, 1–27. https://doi.org/10.2166/aqua.2021.146.

Gizaw, A., Zewge, F., Chebude, Y., Tesfaye, M. & Mekonnen, A. 2021b Phosphate abatement using calcium silicate hydrate synthesized from alum factory solid waste residue. *Sep. Sci. Technol.* **57**, 1–19. https://doi.org/10.1080/01496395.2021.1998125.

Golie, W. M. & Upadhyayula, S. 2016 Continuous fixed-bed column study for the removal of nitrate from water using chitosan/alumina composite. *J. Water Process Eng.* **12**, 58–65. https://doi.org/10.1016/j.jwpe.2016.06.007.

He, Y., Lin, H., Dong, Y., Liu, Q. & Wang, L. 2016 Simultaneous removal of phosphate and ammonium using salt–thermal-activated and lanthanum-doped zeolite: fixed-bed column and mechanism study. *Desalin. Water Treat.* **57**, 27279–27293. https://doi.org/10.1080/19443994.2016.1166459.

Hu, A., Ren, G., Che, J., Guo, Y., Ye, J. & Zhou, S. 2019 Sciencedirect phosphate recovery with granular acid-activated neutralized red mud : fixed-bed column performance and breakthrough curve modeling. *J. Environ. Sci.* **90**, 78–86. https://doi.org/10.1016/j.jes.2019.10.018.

Husein, D. Z., Al-Radadi, T. & Danish, E. Y. 2017 Adsorption of phosphate using alginate-/Zirconium-Grafted newspaper pellets: fixed-bed column study and application. *Arab. J. Sci. Eng.* **42**, 1399–1412. https://doi.org/10.1007/s13369-016-2250-z.

Hussain, T. S. & Al-Fatlawi, A. H. 2020 Remove chemical contaminants from potable water by household water treatment system. *Civ. Eng. J.* **6**, 1534–1546. https://doi.org/10.28991/cej-2020-03091565.

Jang, J. & Lee, D. S. 2019 Effective phosphorus removal using chitosan/Ca-organically modified montmorillonite beads in batch and fixed-bed column studies. *J. Hazard. Mater.* **375**, 9–18. https://doi.org/10.1016/j.jhazmat.2019.04.070.

Jung, K. W., Jeong, T. U., Choi, B. H., Jeong Kang, H. & Ahn, K. H. 2017a Phosphate adsorption from aqueous solution by Laminaria japonica-derived biochar-calcium alginate beads in a fixed-bed column: experiments and prediction of breakthrough curves. *Environ. Prog. Sustainable Energy* **36**, 1365–1373. https://doi.org/10.1002/ep.12580.

Jung, K. W., Jeong, T. U., Choi, J. W., Ahn, K. H. & Lee, S. H. 2017b Adsorption of phosphate from aqueous solution using electrochemically modified biochar calcium-alginate beads: batch and fixed-bed column performance. *Bioresour. Technol.* **244**, 23–32. https://doi.org/10.1016/j.biortech.2017.07.133.

Kuwahara, Y. & Yamashita, H. 2017 Phosphate removal from aqueous solutions using calcium silicate hydrate prepared from blast furnace slag. *ISIJ Int.* **57**, 1657–1664. https://doi.org/10.2355/isijinternational.ISIJINT-2017-123.

Lee, C. G., Kim, J. H., Kang, J. K., Kim, S. B., Park, S. J., Lee, S. H. & Choi, J. W. 2015 Comparative analysis of fixed-bed sorption models using phosphate breakthrough curves in slag filter media. *Desalin. Water Treat.* **55**, 1795–1805. https://doi.org/10.1080/19443994.2014.930698.

Leng, L., Zhang, J., Xu, S., Xiong, Q., Xu, X., Li, J. & Huang, H. 2019 Meat & bone meal (MBM) incineration ash for phosphate removal from wastewater and afterward phosphorus recovery. *J. Cleaner Prod.* **238**, 117960. https://doi.org/10.1016/j.jclepro.2019.117960.

Li, N., Ren, J., Zhao, L. & Wang, Z. L. 2013 Fixed bed adsorption study on phosphate removal using nanosized FeOOH-modified anion resin. *J. Nanomater.* **2013**, 1–6. https://doi.org/10.1155/2013/736275.

Liu, R., Chi, L., Wang, X., Sui, Y., Wang, Y. & Arandiyan, H. 2018 Review of metal (hydr)oxide and other adsorptive materials for phosphate removal from water. *J. Environ. Chem. Eng.* **6**, 5269–5286. https://doi.org/10.1016/j.jece.2018.08.008.

Monfet, E., Aubry, G. & Ramirez, A. A. 2017 Nutrient removal and recovery from digestate : a review of the technology. **7269**, 0–16. https://doi.org/10.1080/17597269.2017.1336348.

Nguyen, T. A. H., Ngo, H. H., Guo, W. S., Pham, T. Q., Li, F. M., Nguyen, T. V. & Bui, X. T. 2015 Adsorption of phosphate from aqueous solutions and sewage using zirconium loaded okara (ZLO): fixed-bed column study. *Sci. Total Environ.* **523**, 40–49. https://doi.org/10.1016/j.scitotenv.2015.03.126.

Nigussie, W., Zewge, F. & Chandravanshi, B. S. 2007 Removal of excess fluoride from water using waste residue from the alum manufacturing process. *J. Hazard. Mater.* **147**, 954–963. https://doi.org/10.1016/j.jhazmat.2007.01.126.

Nuryadin, A. & Imai, T. 2021 Application of amorphous zirconium (hydr)oxide/MgFe layered double hydroxides composite in fixed-bed column for phosphate removal from water. *Global J. Environ. Sci. Manag.* **7**, 485–502. https://doi.org/10.22034/gjesm.2021.04.01.

Pap, S., Kirk, C., Bremner, B., Turk Sekulic, M., Shearer, L., Gibb, S. W. & Taggart, M. A. 2020 Low-cost chitosan-calcite adsorbent development for potential phosphate removal and recovery from wastewater effluent. *Water Res.* **173**, 115573. https://doi.org/10.1016/j.watres.2020.115573.

Pham, T. H., Lee, K. M., Kim, M. S., Seo, J. & Lee, C. 2019 La-modified ZSM-5 zeolite beads for enhancement in removal and recovery of phosphate. *Microporous Mesoporous Mater.* **279**, 37–44. https://doi.org/10.1016/j.micromeso.2018.12.017.

Prashantha Kumar, T. K. M., Mandlimath, T. R., Sangeetha, P., Revathi, S. K. & Ashok Kumar, S. K. 2018 Nanoscale materials as sorbents for nitrate and phosphate removal from water. *Environ. Chem. Lett.* **16**, 389–400. https://doi.org/10.1007/s10311-017-0682-7.

Ramirez, A., Giraldo, S., García-Nunez, J., Flórez, E. & Acelas, N. 2018 Phosphate removal from water using a hybrid material in a fixed-bed column. *J. Water Process Eng.* **26**, 131–137. https://doi.org/10.1016/j.jwpe.2018.10.008.

Reinhardt, T., Rott, E., Schneider, P. A., Minke, R. & Schönberger, H. 2021 Fixed-bed column studies of phosphonate and phosphate adsorption on granular ferric hydroxide (GFH). **153**, 301–310. https://doi.org/10.1016/j.psep.2021.07.027.

Rout, P. R., Bhunia, P. & Dash, R. R. 2017 Evaluation of kinetic and statistical models for predicting breakthrough curves of phosphate removal using dolochar-packed columns. *J. Water Process Eng.* **17**, 168–180. https://doi.org/10.1016/j.jwpe.2017.04.003.

Samaraweera, H., Edwards, J., Reid, C., Perera, S. S., Venkatesh, R., Thirumalai, K. G., Pittman, C. U. & Mlsna, T. 2021 Pyrolyzed Ca-impregnated lignite for aqueous phosphate removal : batch and column studies. *J. Environ. Chem. Eng.* **9**, 106077. https://doi.org/10.1016/j.jece.2021.106077.

Sellner, B. M., Hua, G. & Ahiablame, L. M. 2019 Fixed bed column evaluation of phosphate adsorption and recovery from aqueous solutions using recycled steel byproducts. *J. Environ. Manage.* **233**, 595–602. https://doi.org/10.1016/j.jenvman.2018.12.070.

Singh, D. K., Kumar, V., Mohan, S., Bano, D. & Hasan, S. H. 2017 Breakthrough curve modeling of graphene oxide aerogel packed fixed-bed column for the removal of Cr(VI) from water. *J. Water Process Eng.* **18**, 150–158. https://doi.org/10.1016/j.jwpe.2017.06.011.

Sun, X. F., Imai, T., Sekine, M., Higuchi, T., Yamamoto, K., Kanno, A. & Nakazono, S. 2014 Adsorption of phosphate using calcined Mg3-Fe layered double hydroxides in a fixed-bed column study. *J. Ind. Eng. Chem.* **20**, 3623–3630. https://doi.org/10.1016/j.jiec.2013.12.057.

Wang, S., Kong, L., Long, J., Su, M., Diao, Z., Chang, X., Chen, D., Song, G. & Shih, K. 2018 Adsorption of phosphorus by calcium-flour biochar: isotherm, kinetic and transformation studies. *Chemosphere* **195**, 666–672. https://doi.org/10.1016/j.chemosphere.2017.12.101.

Woumfo, E. D., Siéwé, J. M. & Njopwouo, D. 2015 A fixed-bed column for phosphate removal from aqueous solutions using an andosol-bagasse mixture. *J. Environ. Manage.* **151**, 450–460. https://doi.org/10.1016/j.jenvman.2014.11.029.

Wu, B., Fang, L., Fortner, J. D., Guan, X. & Lo, I. M. C. 2017 Highly efficient and selective phosphate removal from wastewater by magnetically recoverable $La(OH)_3/Fe_3O_4$ nanocomposites. *Water Res.* **126**, 179–188. https://doi.org/10.1016/j.watres.2017.09.034.

Ye, Y., Wei, Y., Gu, Y., Kang, D., Jiang, W. & Kang, J. 2020 Simultaneous removal of fluoride and phosphate in a continuous fixed-bed column filled with magnesia-pullulan composite. *J. Alloys Compd.* **838**, 155528. https://doi.org/10.1016/j.jallcom.2020.155528.

Ye, J., Yang, M., Ding, X., Tan, W., Li, G., Fang, S. & Wang, H. 2021 Fixed-bed column dynamics of ultrasound and Na-functionalized diatomite to remove phosphate from water. *Environmental Science and Pollution Research* **29**(9), 12441–12449

Zhang, Z., Wang, X. & Zhao, J. 2019 Phosphate recovery from wastewater using calcium silicate hydrate (C-S-H): sonochemical synthesis and properties. *Environ. Sci. Water Res. Technol.* **5**, 131–139. https://doi.org/10.1039/c8ew00643a.

First received 19 December 2021; accepted in revised form 9 July 2022. Available online 19 July 2022